Towards A Flamelet Library Using Bi-orthogonal Interpolating Wavelets

A. J. Lowe* and R. Prosser†

Abstract—**The use of wavelets within a multiresolution framework provides an adaptive Large Eddy Simulation for the investigation of multi-scale phenomena such as premixed turbulent combustion. Within such an approach, we use the flamelet method and model the structure of infinitely thin flames separating the reactants from the product gases. Here we ask the question; how does the selection of a bi-orthogonal wavelet basis affect the structure of a flamelet for both adaptive and non-adaptive simulations? We show the results of expressing a laminar flame profile in terms of a set of wavelet coefficients, and show how the removal of information using two alternative strategies leads to errors. We use bi-orthogonal interpolating wavelets of fourth order. We demonstrate the effect of the removal of individual sub-spaces in a non-adaptive setting and the removal of information based on a simple thresholding strategy typical of an adaptive simulation. We show that both methods can adequately represent the profile to within a specified level of accuracy. Furthermore, the thresholding strategy requires less grid points to attain the same level of accuracy.**

Index Terms—**biorthogonal, flamelets, interpolating wavelets, thresholding .**

I. Introduction

This paper is concerned with the construction of a flamelet library within the framework of multiresolution Large Eddy Simulation using wavelets. Wavelets offer significant benefits in reducing the computational burden of turbulent combustion simulations [11] . Furthermore, fast transforms are available that allow efficient computations in an adaptive setting [14] & [12]. Wavelets have long been used in image processing and are well established as a tool for both the analysis and simulation of physical phenomena, [7],[8],[9],[10]&[11]. For this investigation we use second generation biorthogonal interpolating wavelets [18]. Other types of wavelets are detailed in the more general background reference for wavelets, [5]. Although they do not obey the admissibility condition, they nevertheless provide a useful numerical tool because of their inherent versatility, [6]. With biorthogonal interpolating wavelets we can control the order of interpolation and boundary constructions. The admissibility condition can be satisfied if the wavelets are lifted [15], although this property is not exploited here.

We investigate a laminar diffusion flame on a grid of 512 points. We take the fixed point in the flame and position it at intermediary grid points separating the coarse scaling function points of the grid. Wavelets are not translational invariant, which implies that each grid point is associated with a unique subspace. We use a subtraction based fast wavelet transform to decompose the flame into a coarse resolution scaling function space and detailed wavelet subspaces. We then investigate two strategies for information removal; these are associated with a non-adaptive and an adaptive simulation. In the first instance, information removal is governed by subspace removal, and in the other case by a simple thresholding strategy. The flame is then reconstructed based on the reduced information contained in the subspaces, and the error is measured. We are interested in the special case of where the length scale of the flame approaches that of the LES and indeed where the flame may span more than two coarse scaling function grid points. We do not consider the case of a flame length-scale much less than the LES grid spacing.

II. Wavelets

In bi-orthogonal wavelet systems [13], two scaling function subspaces, V and $\widetilde{V}$, combine to form an approximation of a function. A cascade of spaces, each made up of a primal ($\phi(x)$) and a dual ($\widetilde{\phi}(x)$) basis function, form a hierarchy:

$$V_{j-1} \subset V_j \subset V_{j+1},$$

$$\text{and} \quad \widetilde{V}_{j-1} \subset \widetilde{V}_j \subset \widetilde{V}_{j+1}.$$

j represents a resolution of 2^j grid points, with an associated length-scale of $\sim 2^{-j}$. The detail spaces (or wavelet spaces) W and $\widetilde{W}$ complete the bi-orthogonal set. A Primal wavelet ($\psi(x)$)and a dual wavelet ($\widetilde{\psi}(x)$) function form the basis of the hierarchy of wavelet spaces. Spaces are combined such that,

$$V_{j+1} = V_j \oplus W_{j+1},$$

$$\widetilde{V}_{j+1} = \widetilde{V}_j \oplus \widetilde{W}_{j+1}.$$

Also, $\widetilde{V}_j$ is orthogonal to W,

$$\widetilde{V} \perp W,$$

and V_j is orthogonal to $\widetilde{W}_j$,

$$V \perp \widetilde{W}.$$

The Authors are grateful to the UK Engineering and Physical Sciences Research Council for funding.

* University of Manchester, MACE, Manchester, M60 1QD, UK, a.lowe-3@manchester.ac.uk.
† University of Manchester, MACE, Manchester, M60 1QD, UK, robert.prosser@manchester.ac.uk.

Prosser [12], shows a fast wavelet transform that provides a coarse scale, at the resolution of *J-m, m>0*, and 'detail' wavelet coefficients at resolutions *J-m* to *J-1*. Here, *J* is the finest resolution with 2^J+1 grid points. Both sets of coefficients reconstruct the original function via the inverse transform. The projection of a function onto the coarse and detail spaces follows from,

$$P_j(f(x)) = \sum_k \left\langle f(u), \tilde{\phi}_{j,k}(u) \right\rangle \phi_{j,k}(x),$$

$$Q_j(f(x)) = \sum_k \left\langle f(u), \tilde{\psi}_{j,k}(u) \right\rangle \psi_{j,k}(x),$$

with <·,·> the inner product.

Second Generation wavelets form a more general framework for the construction of wavelets, [15], [16] & [17]. Here, we adopt the biorthogonal interpolating wavelets of [18]. In contrast to the filtering approach of LES, wavelet based multiresolution LES, for example, decomposes the velocity such that,

$$u(x) = P_{J-m}(u) \oplus \sum_{i \geq J-m} Q_i\ (u),$$

where the coarse resolved and retained scale is projected onto $V_{J\text{-}m}$. In both the adaptive and non adaptive setting, we retain the coarse scale projection ($P_{J\text{-}m}$) and remove some if not all of the wavelet sub spaces, W_i. All unresolved and removed spaces would be modeled based on a statistical approach. The statistical modeling is analogous to a sub grid scale model. We note here that we would expect a typical flame to be significantly smaller than the resolution of the coarsest scale. However, our investigation looks at a flame that spans the coarsest resolution, *J-m*. In doing so, we establish the need for the flame thickness to be significantly smaller than the finest resolved scale and highlight the need for adequate resolutions should the LES approach a DNS (where the flame is fully resolved). The wavelet transforms and their use in the investigation of turbulence is covered in [7], [8] & [9]. In LES, wavelets have been used for adaptive simulations in [10].

III. Governing Equations

The governing equations for a typical combustion problem are continuity, momentum, energy and progress variable (*c*) are in Cartesian form:

$$\frac{\partial \rho}{\partial t} + \frac{\partial (\rho u_j)}{\partial x_j} = 0,$$

$$\frac{\partial \rho u_i}{\partial t} + \frac{\partial (\rho u_i u_j + p)}{\partial x_j} = \frac{\partial (\tau_{ij})}{\partial x_j},$$

$$\frac{\partial \rho E}{\partial t} + \frac{\partial (u_j(\rho E + p))}{\partial x_j} = -\frac{\partial q_j}{\partial x_j} + \frac{\partial (u_i \tau_{ij})}{\partial x_j},$$

$$\frac{\partial (\rho c)}{\partial t} + \frac{\partial (\rho u_j c)}{\partial x_j} = \dot{\omega}_c + \frac{\partial}{\partial x_j}\left(\rho D \frac{\partial (c)}{\partial x_j} \right),$$

where, ρ is density, *u* is velocity, *p* is pressure, *q* is heat flux, *Y* is the species mass fraction, *D* is the mass diffusion coefficient and *E* the energy. In premixed combustion analysis, we use a progress variable *c* to track the chemical reactions between reactants and products. *c* is defined via,

$$c = \frac{Y_p - Y_{po}}{Y_{p\infty} - Y_{po}},$$

with Y_p, the mass fraction of product species, and the subscripts *o* and ∞ represents the fresh and product gases respectively. Typically, we adopt a single-step chemistry reaction mechanism based on the Arrhenius reaction rate, $\dot{\omega}$,

$$\dot{\omega} = B^* \rho (1-c) \exp\left[\frac{\beta(1-\hat{T})}{1-\alpha(1-\hat{T})} \right].$$

Here, β is the Zel'Dovitch number, ρ the density, B^* is the normalised preexponential factor and α the heat release parameter. The non-dimensional temperature is defined as

$$\hat{T} = \frac{T - T_o}{T_\infty - T_o}.$$

Numerical simulations investigating the progress variable can be found for Direct Numerical Simulations (DNS) in [1], [21] and [3] and Large Eddy Simulations (LES) in [19] and [20].

The flamelet approach used in modeling combustion is well established, [2]. It assumes that combustion takes place in a laminar, infinitely thin strip or infinitely thin surface in 3D. Conveniently, our assumption disassociates the direct effects of turbulence on the combustion but retains the turbulent deformation of the flamelet layer or surface. At this point, we draw on the flamelet library to describe the profile of the progress variable. Our library would typically include profiles based on, for example, radius of curvature K_m, or tangential strain rate a_T, etc. A mathematical description of surfaces in turbulent flows can be found in, [4]. Investigation of progress variable iso-surfaces can be found in, [23], with specific numerical investigations in [1]&[3] and experimental investigation in [22]. A comprehensive review of flamelets in non-premixed combustion can be found in [2].

Our paper is not concerned with construction of the library itself; instead, we are faced with the question of how the interpolating bi-orthogonal wavelet representation of the flamelet introduces errors. We define a progress variable value of c^*, an isosurface where the infinitely thin flamelet is assumed to be located.

Fig. 1 shows the 1D laminar flame solution profile of *c* on a 512 node grid, for a domain of 1.8mm, with a Zel'Dovitch number of 6, heat release parameter of 0.6 and preexponential factor of $285100s^{-1}$. We note here that this is a typical form of the profile, [24].

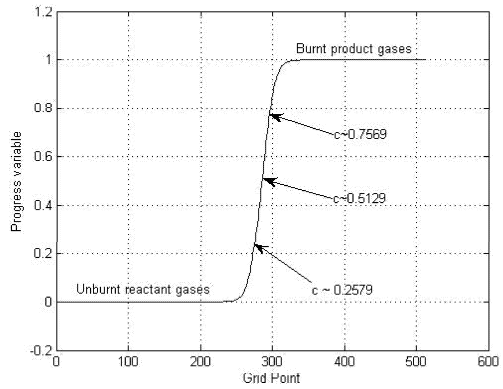

Fig. 1: Profile of progress variable, c, on 512 grid points, n. Arrows locate the c^* values of 0.2579, 0.5129 and 0.7569.

IV. Method

From the profile defined in the III, we shall apply a 1D wavelet transform via successive subtraction to give,

$$P_J(c(x)) = P_{J-m}(c(x)) \oplus \sum_{i=J-m}^{J-1} Q_i(c(x)),$$

and remove coefficients based on one of the following strategies:

1. successively removing entire wavelet subspaces, $W_i(c(x))$.
2. setting wavelet coefficients less than a particular threshold, ξ (see Table I) , to zero.

We then perform an inverse transform on the subset of coefficients and analyse the new profile, c'.

In doing so, we shall measure the maximum error, ε, defined as

$$\varepsilon = \sum_{i=0}^{n} |c_i' - c_i|,$$

where n is the retained set of points after removal of points. We repeat this exercise by translating the progress variable profiles across two coarse scale grid points by placing the profiles at a grid point associated with each wavelet subspace, $4 \le j \le 8$. Table II shows the range of subspaces and locations over which the progress variable profile is translated. Again, we note that the wavelets are not translational invariant and each grid point is associated with a wavelet subspace. We see in Table II that each point is associated with a wavelet subspace. When the flame profile is placed on that grid point, the wavelet coefficient will be relatively large compared to that when the flame is translated onto another grid point associated with another wavelet subspace. This example highlights one of the non-linear errors that a strategy for wavelet coefficient removal must address.

Table I: Threshold values.

Ref.	ξ
i)	10^{-1}
ii)	10^{-2}
iii)	10^{-3}
iv)	10^{-4}
v)	10^{-5}
vi)	10^{-6}

Table II: Subspace reference location and nodes.

Ref.	Subspace	Resolution, j.	Grid point.
a)	V_4	4	256
b)	W_4	4	240
c)	W_5	5	248
d)	W_6	6	252
e)	W_7	7	254
f)	W_8	8	255

V. Results

Here we present the results representing a typical flamelet progress variable profile; we systematically increase the level of detail captured by fourth order bi-orthogonal interpolating wavelets based on two simple strategies. Table III shows the number of grid points retained and error, ε. The progress variable value is $c^* \sim 0.5$ and complete sets of subspace wavelets coefficients are removed. Table IV shows the number of grid points retained and error, ε. The progress variable value is $c^* \sim 0.5$. Wavelets coefficients are removed based the thresholds, i)-vi). We have not included the data for the profiles located around progress variable values $c^* \sim 0.25$ & $^*c \sim 0.75$ as there are no significant differences in trends and conclusions. Furthermore, in Tables III and IV we also include the results from placing on flame profile located around $c^* \sim 0.5$ on grid points a)-f).

We see that in relatively coarse profile approximations ($V_4 \oplus W_4$), the magnitude of the error depends on the initial placing of the profile. In both the thresholded and subspace coefficient removal strategies, we then see the errors, ε converge to order $\sim 10^{-3}$ for a threshold of 10^{-4} and the retention of three wavelet subspaces. The subspace removal strategy retains approximately three times more grids points than the thresholding strategy. In other words, the thresholding strategy takes the advantage of requiring less grid points for errors of the same order of magnitude. We also note in passing that the error scales with threshold. We see in Fig. 2 that relatively high magnitude thresholds give unphysical values of progress variable; for a threshold of 0.01, the profile has both undershoot, $c<0$, and overshoot, $c>1$. For a threshold of 10^{-4} the profile compares well with the original progress variable profile, Fig 1, with no over or under shoot.

Table III : Error norm for wavelet removal strategy using subspace removal.

Subspaces retained **(Grid Points retained in brackets)**	Error norm, profile location, *a)-f)*. a)	b)	c)	d)	e)	f)
V_4 ***(17)***	5.0454	0.7902	3.4763	4.6006	4.9147	5.0033
$V_4 \oplus W_4$ ***(33)***	0.3623	0.3623	0.4268	0.4862	0.4425	0.4043
$V_4 \oplus W_4 \oplus W_5$ ***(65)***	0.295	0.0295	0.0295	0.0342	0.0305	0.0283
$V_4 \oplus \sum_{i=4}^{6} W_i$ **(129)**	0.022	0.0022	0.0022	0.0022	0.0022	0.0022
$V_4 \oplus \sum_{i=4}^{7} W_i$ ***(257)***	0.0001	0.0001	0.0001	0.0001	0.0001	0.0001
$V_4 \oplus \sum_{i=4}^{8} W_i$ ***(513)***	$7.36\ 10^{-15}$	$1.27\ 10^{-14}$	$1.11\ 10^{-14}$	$7.43\ 10^{-15}$	$8.97\ 10^{-14}$	$1.11\ 10^{-14}$

Table IV : Error norm for wavelet removal strategy using thresholds i) – vi).

Threshold	Error norm, profile location, *a)-f)*. **(Grid Points retained in brackets)** a)	b)	c)	d)	e)	f)
i)	3.0142**(18)**	0.7902**(17)**	3.4763**(17)**	4.6006**(17)**	4.9147**(17)**	3.0457**(18)**
ii)	0.2600**(22)**	0.5935**(19)**	0.3216**(22)**	0.3311**(22)**	0.2995**(22)**	0.2764**(22)**
iii)	0.0577**(27)**	0.0325**(28)**	0.0262**(30)**	0.0261**(32)**	0.0362**(30)**	0.0461**(28)**
iv)	0.0031**(44)**	0.0053**(43)**	0.0028**(45)**	0.0035**(44)**	0.0038**(43)**	0.0040**(42)**
v)	0.0005**(71)**	0.0003**(72)**	0.0003**(73)**	0.0004**(72)**	0.0006**(69)**	0.0005**(71)**
vi)	0.000041**(116)**	0.000062**(115)**	0.000044**(117)**	0.000044**(118)**	0.000040**(117)**	0.000043**(118)**

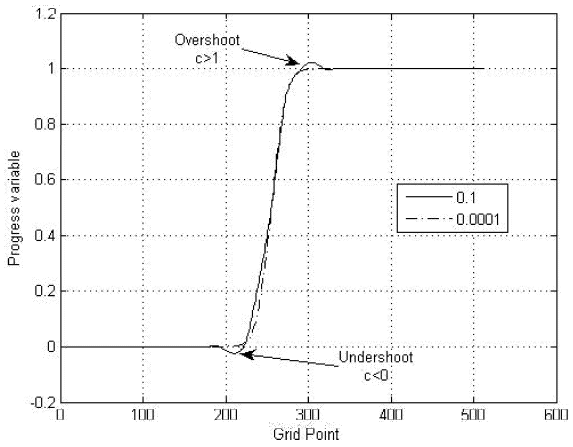

Fig 2: The profiles of progress variable, *c*, from the thresholding reduction strategy with $\xi=10^{-1}$ and $\xi=10^{-4}$. The profile is located on grid point 256, here the progress variable focal point is *c* ~0.5.

Fig 3 and Fig 4 show the decay of error against threshold and retained subspaces for progress variable profiles (*c~0.25, c~0.50 & c~0.75*) located on grid point 256.

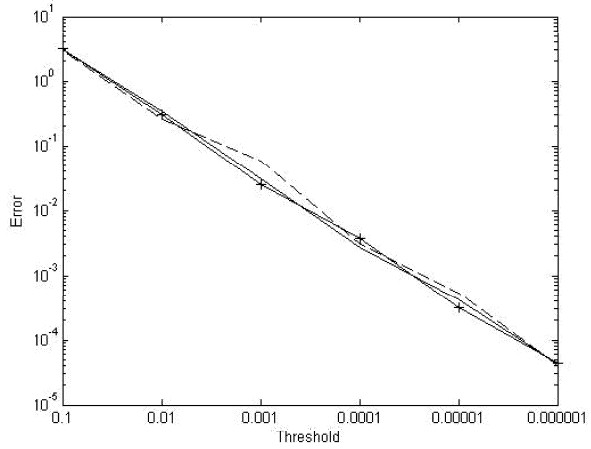

Fig 3: Error plotted against threshold, ξ. With *c~0.25* (solid), *c~0.50* (dash dash) and *c~0.75* (solid +) .

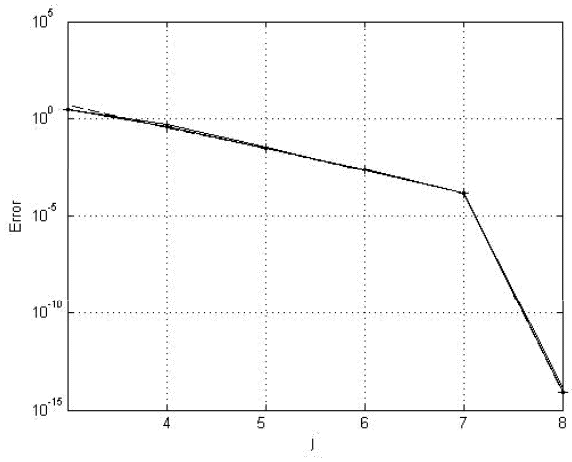

Fig 4: Error plotted against subspaces retained, *j*, such that $c'(x) = V_{J-m}(c(x)) \oplus \sum_{i=J-m}^{j} W_i\ (c(x))$. With *c~0.25* (solid), *c~0.50* (dash dash) and *c~0.75* (solid +) .

VI. Conclusion

The conclusion of this paper is that both subspace removal and thresholding are viable strategies for the removal of biorthogonal interpolating wavelet coefficients. In addition, the thresholding strategy requires less grid points. Future work will develop a wavelet based library extracted from DNS databases taking into account turbulent physical characteristics. This work has highlighted the need for care when developing LES simulations where the resolution of the grid is approaching that of a DNS simulation and the flame spans the coarse grid resolution.

References

[1] N. Chakraborty & R. S. Cant. Unsteady effects of strain rate and curvature on turbulent premixed flames in an inflow-outflow configuration. Combustion and Flame 137 (2004) 129-147.

[2] N. Peters. Laminar diffusion flamelet models in non-premixed turbulent combustion. Prog. Energy Combust. Sci., 1984, Vol. 10, pp. 319-339.

[3] N. Chakraborty & R. S. Cant. Effects of strain rate and curvature on surface density function transport in turbulent premixed flames in the thin reaction zones regime. Physics of Fluids 7, 065108 (2005).

[4] S. B. Pope, The evolution of surfaces in turbulence, Int. J. Eng. Sci. 26(5), 445 (1998).

[5] I. Daubechies, Ten lectures on wavelets, SIAM, Philadelphia, 1992, CBMS Lecture Notes, No 61.

[6] R. Prosser, On the effects of lifted wavelets for combustion simulations, submitted for publication, 2006.

[7] M. Farge, Wavelet Transforms and Their Applications To Turbulecnce, Ann. Rev. Fluid Mech. 24 (1992) 395-457.

[8] M. Farge, G. Pellegrino, K. Schneider, Coherent Vortex Extraction in 3D Turbulent Flows Using orthognoal Wavelets, Phys. Rev. Lett. 87 (2001) 1-4.

[9] M. Farge, K. Schneider, N. Kevlahan, Non- Gaussianity and Coherent Vortex Simulation for Two Dimensional Turbulence Using an Adaptive Orthogonal Wavelet Basis, Phys. Fluids A 11 (1999) 2187.-2201.

[10] D. Goldstein, O. Vasilyev, Stochastic Coherent Adaptive Large Eddy Simluation Method, Phys. Fuids 16 (2004) 2497-2513.

[11] R. Prosser, Numerical Methods for the Computation of Combustion, Ph.D. thesis, Cambridge University (1997).

[12] R. Prosser, A Fourth Order Wavelet Based Adaptive Algorithm for Compressible Reacting Flows, Preprint (2006).

[13] A. Cohen, I. Daubechies, J. Feauveau, Biorthogonal Bases of Compactly Supported Wavelets, Commun. Pure Appl. Math. 45 (1992) 485-560.

[14] A. Cohen, I. Daubechies, P. Vial, ,Wavelets on the Interval and Fast Wavelet Transforms, Appl. Comp Harmonic Analysis 1 (1993) 54-81.

[15] W. Sweldens, The Lifting Scheme: A Custom Design Construction of Biorthogonal Wavelets, Appl. Compu. Harm. Anal. 3 (1996) 186-200.

[16] W. Sweldens, The Lifting Scheme: A Construction of Second Generation Wavelets, SIAM J. Math. Anal. 29 (1997) 511-546.

[17] P. Schröder, W. Sweldens, Building Your Own Wavelets at Home, in: ACMSIGGRAPH Course Notes, 1996.

[18] D. Donoho, Interpolating Wavelet Transforms, Presented at The NATO Advanced Study Institute Conference on 'Wavelets and Applications,' II Ciocco, Italy (August 1992).

[19] E. R. Hawkes, Large Eddy Simulation of premixed turbulent combustion, Ph.D. thesis University of Cambridge, Engineering Department, UK 2000.

[20] E. R. Hawkes and R. S. Cant, Implications of a flame surface density approach to LES of turbulent premixed combustion, Combust. Flame 126, 1617 (2001).

[21] R. S. Cant, Direct Numerical Simulation of premixed turbulent flames, Philos. Trans. R. Soc. London, Ser A 357, 3583 (1999).

[22] D. Veynante, J. M. Duclos, and J. Piana, Experimental analysis of flamelet models for premixed turbulnet combustion. Proc. Combust. Inst. 25, 1249 (1994).

[23] N. Peters, Turbulent combustion, Cambridge University Press, Cambridge, 2000.

[24] F. Williams, Combustion Theory - Second Edition, Perseus Books, ISBN 0-8053-9801-5, 1985.